Linking scale-specific sinuosity to hydrogeomorphic domains in Alaska watersheds

Lawrence V. Stanislawski [1]*, Pierfranco Costabile [2], Barry J. Kronenfeld [3], and Margherita Lombardo [2]

[1] U.S. Geological Survey, Center of Excellence for Geospatial Information Science, Rolla, Missouri, United States
[2] Department of Environmental Engineering, University of Calabria, Rende, CS, Italy
[3] Department of Geology and Geography, Eastern Illinois University, Charleston, Illinois, United State
* lstan@usgs.gov

Keywords: elevation model, sinuosity, hydrography, geomorphology, inundation pattern domain

Introduction

River meander patterns arise from geomorphological processes influenced by climate, geology, terrain, and hydrology. These processes produce a wide spectrum of sinuous channel and meander forms, and understanding them is essential for land management practices, such as natural channel restoration (Dominguez et al., 2018), flood and erosion control, bank stabilization (U.S. Department of Interior, 2015), and riparian corridor and agricultural land management (Ran, et al., 2022; Yu, et al., 2023; Zhu et al., 2022). Studies of meander migration provide insight into sediment dynamics and river ecosystem health (Ielpi et al. 2023, Constantine et al., 2014). A river's natural ability to clean itself, or reduce pollutants, through physical, chemical, and biological processes, also termed self-purification capacity, has been linked to river sinuosity (Xiao et al, 2019, 2025).

Scale-specific sinuosity (S3) is an easily computed metric for characterizing planform meander bend geometry across a range of measurement scales (Stanislawski et al., 2023). Unlike the traditional single summary value of sinuosity for a stream section, S3 estimates the relative distribution of meander-bend sizes, such as peak-to-trough lengths, within a planform linear representation of a stream section, along with the relative contributions of these bend sizes to its overall sinuosity. The aim of this study is to assess the potential of S3 as a diagnostic geomorphic metric with applications to process-based river and fluvial domain classification.

Rivers vary widely in their sensitivity to change depending on sediment and bedload materials, landscape position, and hydroclimatic variability, including flooding or drought. River classification systems were developed to organize the diversity of river forms and processes in ways that support both scientific understanding and management needs. Classification provides a framework for geomorphological analyses related to resource assessment, habitat evaluation, and mitigation of natural or human-driven disturbances. Process-based classification systems help predict how channels respond to changes in flow or sediment regimes (Buffington and Montgomery, 2022), and also support resource exploration because ecological habitats, mineral deposits, and other natural resources often correspond to sediment characteristics that vary systematically across channel types (Rosgen, 1994; Wheaton et al., 2013; Wheaton et al., 2015). Planform-based metrics such as channel sinuosity have long been components of river classification systems (Rosgen, 1994; Wheaton et al., 2015; Buffington and Montgomery, 2022), where sinuosity is measured as a simple ratio of path length over end-to-end distance.

A general model for stream sinuosity indicates that sinuosity is related to the ratio of terrain slope to substrate resistivity (Lazarus and Constantine, 2013), although low-slope, valley, and flood plain environments exhibit a broader range of sinuosity values than high-slope conditions. Variability in channel pattern morphology is governed by the physics of fluvial processes and eight stream channel properties, which include channel width, depth, velocity, discharge, channel slope, roughness of channel materials, sediment load, and sediment size (Leopold et al., 1964). Traditional planform meander-bend geometry metrics typically collapse complex meander patterns into one or more measures, such as sinuosity, meander wavelength, frequency, or amplitude (Tallar et al., 2023). However, rivers express meander patterns across a range of spatial scales, from high-frequency small bends in steep headwaters to low-frequency large meanders in low-relief floodplains. Consequently, this scale diversity means similar overall sinuosity values can arise from fundamentally different geomorphic settings, limiting the diagnostic power of conventional single summary sinuosity measures.

Research by Costabile et al. (2024) applied a hydrodynamic hierarchical framework to identify inundation pattern domains (IPDs) within watersheds using digital elevation model (DEM)-derived two-dimensional shallow water models driven by rain-on-grid forcing. The IPDs delineate distinct hydrogeomorphic domains such as hillslope, unchanneled valleys, and flood plains within the 12-digit hydrologic unit (HU12) watersheds (U.S. Geological Survey, 2023) in the Kobuk River valley in northcentral Alaska. S3 can be aggregated to produce average meander distributions for IPDs, such as unchanneled secondary branches and low-relief floodplain valleys, enabling comparisons across domains. In this way, S3 provides an easily comparable metric for summarizing meander bend sinuosity patterns across hydrogeomorphic and broader geophysical contexts.

In this work, we use S3 plots to assess channel sinuosity across IPDs within Alaskan watersheds using 1:24,000-scale vector hydrography and 5-meter (5-m) resolution DEMs derived from Interferometric Synthetic Aperture Radar (IfSAR) data. The objective of this study is to evaluate whether S3 meander signatures differ systematically across IPDs in Alaska watersheds and whether S3 can help distinguish geomorphic process environments at the watershed scale to support process-based river classification.

Methods

In this work, HU12 watersheds are subdivided into riverbed and hillslope (or mountain) domains using the last (rightmost) scale break identified for the unit discharge to watershed drainage density (WDD) curve derived by methods described by Costabile et al. (2024), with scale breaks found by Feldmann et al. (2026) methods. Figure 1 demonstrates the use of the unit discharge value of 0.5 square meters per second (m^2/sec) as a threshold to subdivide HU12 watershed 190503021109 into the welldefined main channel reaches within the flood plain from the more ephemeral and peripheral channel segments and the surrounding hillslope domain. Figure 1b shows this 0.5 m^2/sec threshold value on the WDD to unit discharge curve.

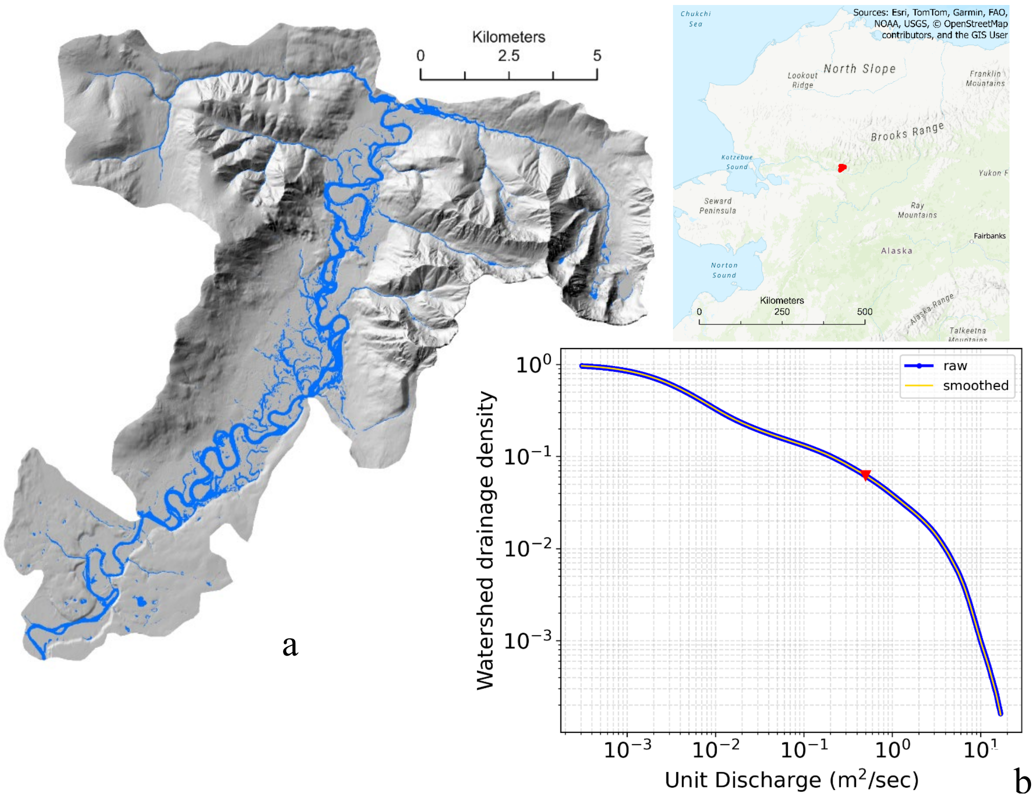

Figure 1: a) Main channels within the flood plain of 12-digit hydrologic unit (HU12) watershed 190503021109 overlaid on grey hill-shaded digital elevation model. The blue area has flow discharge greater than or equal to 0.5 m^2/sec. The index map at the right shows the location of the watershed in red. b) The watershed drainage density to unit discharge curve, with the 0.5 minimum discharge threshold (marked with a red triangle) that separates the main channels and hillslope domains.

Using custom Python and open-source tools, S3 analysis is applied to 1:24,000-scale elevation-derived hydrography (EDH) generated from 2012-2013 IfSAR data compiled for the U.S. Geological Survey (USGS) 3D Hydrography Program (USGS, 2026). The IfSAR dataset includes 5-m resolution DEMs from the USGS 3D Elevation Program (USGS, 2017). Vector channel features in the EDH drainage network are assembled into connected flow paths, ordered from longest to shortest within each HU12 watershed. These connected paths form the basis for S3 computations.

For each path, an average S3 plot is computed from a sliding window that covers about 10 meters less than the window that encompasses the entire path. Window start locations are randomly selected. The stride range of the window is subdivided into a number of bins that depends on the window size. A fixed bin size is selected based on the lengths of the paths in the dataset. A random sample of stride lengths is selected for each bin. For each window, strides lengths are sorted in increasing order, and an S3 plot is generated by incrementally computing the slope of the Richardson plot across successively increasing stride lengths, where the Richardson plot represents path length measured using progressively larger stride lengths (see Stanislawski et al., 2023 for details). Average and standard deviation S3 values are compiled for all stride bins in all windows, possibly excluding the largest stride bins if the minimum number of observations is not found. A 95 percent confidence interval is computed for each bin. Figure 2a shows the S3 plot for the longest path in HU12 190503021109, which lies within the floodplain IPD, while Figure 2b shows an S3 plot for a hillslope path.

Subsequent analysis compares S3 signatures aggregated by IPD and by watershed. The fixed bin size allows statistical summaries of S3 values to be computed and compared both by bin and by complete S3 signature. However, differing ranges of path lengths between domains limit comparisons to the common bin ranges.

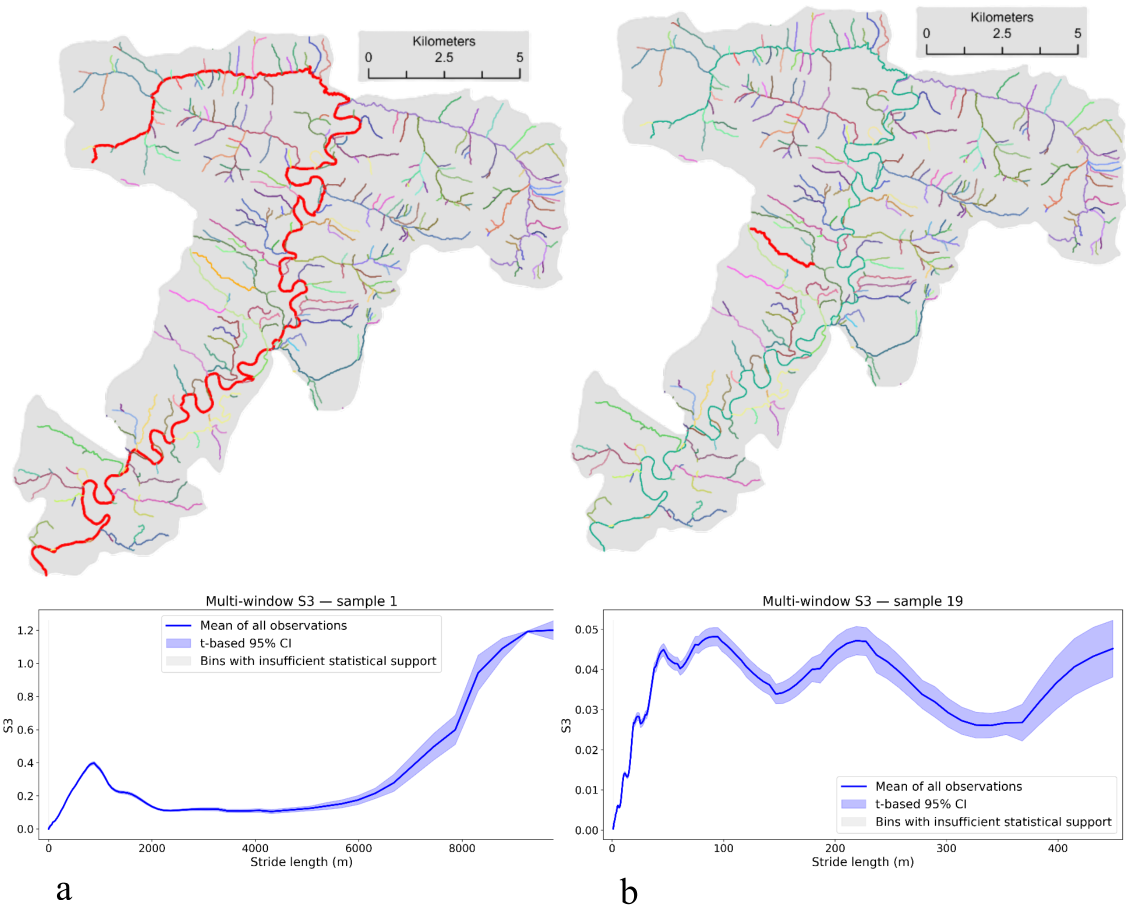

Figure 2: Multi-colored paths delineated for the elevation-derived hydrography channel network collected for 12-digit hydrologic unit (HU12) watershed 190503021109, a) main path #1 (bold red) within the flood-plain domain and the associated multi-window average scale-specific sinuosity (S3) plot for path #1, and b) path #19 (bold red) from the hillslope domain and the associated multi-window average S3 plot. 95 percent confidence intervals for each average are shaded in light blue. S3 signatures quantify variations in meander patterns and sinuosity across different fluvial domains.

Discussion

S3 analysis provides a new way to evaluate stream meander patterns by quantifying how sinuosity varies across multiple spatial scales. This multi-scale perspective enables comparisons of meander geometry across different fluvial environments and geophysical settings. This work demonstrates how S3 metrics and signatures differ between a more sinuous main channel and a straighter secondary channelization associated with an unchanneled mountain valley. This comparison highlights the potential of S3 to characterize and distinguish different hydrogeomorphic configurations within the channel domain. S3 signatures in Figure 2 indicate that meander bends ranging in length from approximately 100 to 10,000 m contribute to relatively higher sinuosity in the main-channel path, whereas smaller bends, ranging from approximately 10 to 500 m, characterize the straighter secondary channelization within the unchanneled valley.

One focus of this work assesses the statistical variability of watershed-based S3 meander signatures and whether differences in S3 distributions can be linked to terrain conditions, including variations in fluvial processes, permafrost influence, or underlying geology. As the analysis expands to additional watersheds, we expect to refine the statistical characterization of S3 signatures and evaluate their potential for supporting process-based river classification.

Disclaimer: Any use of trade, firm, or product names is for descriptive purposes only and does not imply endorsement by the U.S. Government.

References

Buffington, J. M.; Montgomery, D. R. (2022). Geomorphic classification of rivers: An updated review. In: Shroder, John (Jack) F., ed. Treatise on Geomorphology (Second Edition). Academic Press. p. 1143-1190. Retrieved from https://research.fs.usda.gov/treesearch/63526

Costabile, P., Costanzo, C., Lombardo, M., Shavers, E., & Stanislawski, L. V. (2024). Unravelling spatial heterogeneity of inundation pattern domains for 2D analysis of fluvial landscapes and drainage networks. Journal of Hydrology, 632, 130728.

Constantine, J., Dunne, T., Ahmed, J., Legleiter, C., Lazarus, E.D. (2014). Sediment supply as a driver of river meandering and floodplain evolution in the Amazon Basin. Nature Geosci 7, 899–903. https://doi.org/10.1038/ngeo2282

Dominguez, L., Gutierrez, R., Ponte, Y., Abad, J.D., Carrera, O. (2018). Dynamic characterization of meandering channel planform. E3S Web of Conferences 40 (2018), 02043. https://doi.org/10.1051/e3sconf/20184002043.

Falgout, J.T., Gordon, J., Davis, M.J. (2026). USGS Advanced Research Computing, USGS Tallgrass Supercomputer: U.S. Geological Survey, https://doi.org/10.5066/P9XE7ROJ

Feldmann, D., Laux, P., Heckl, A, Nujić, M., Böker, B., Schindler, M., Kunstmann, H. (2026). Sensitivity and scale dependence of discretization and roughness in the hydrodynamic modelling of surface runoff caused by rainfall. J. Hydrology, 669(A), https://doi.org/10.1016/j.jhydrol.2026.135088

Ielpi, A., Lapôtre, M.G.A., Finotello, A., Roy-Léveillée, P. (2023). Large sinuous rivers are slowing down in a warming Arctic. Nat. Clim. Chang. 13, 375–381. https://doi.org/10.1038/s41558-023-01620-9

Lazarus E D, and Constantine J A, (2013). Generic theory for channel sinuosity, Proceedings National Academy of Sciences 110(21): 8447-8452

Leopold, L.B., Wolman, M.G., and Miller, J.P., 1964, Fluvial processes in geomorphology, 544 p.

Ran, Y., Liu, Y., Wu, S., Li, W., Zhu, K., Ji, Y., Mir, Y., Ma, M., Huang, P. (2022). A higher river sinuosity increased riparian soil structural stability on the downstream of a dammed river. Science of The Total Environment, 802 (2022), 149886, https://doi.org/10.1016/j.scitotenv.2021.149886.

Rosgen, D.L. (1994). A classification of natural rivers. Catena 22, 169–199.

Stanislawski, L.V., Kronenfeld, B.J., Buttenfield, B.P., Shavers, E.J. (2023). At what scales does a river meander? Scale-specific sinuosity (S3) metric for quantifying stream meander size distribution. Geomorphology, 436. https://doi.org/10.1016/j.geomorph.2023.108734

Wheaton, J., J. Brasington, S. E. Darby, A. Kasprak, D. Sear, and D. Vericat (2013), Morphodynamic signatures of braiding mechanisms as expressed through change in sediment storage in a gravel-bed river, J. Geophys. Res. Earth Surf., 118, 759–779, doi:10.1002/jgrf.20060.

Wheaton. J.M., Fryirs, K.A.,Brierley, G., Bangen, S.G., Bouwes, N., O'Brien, G., (2015). Geomorphic mapping and taxonomy of fluvial landforms, Geomorphology, 248: 273-295. https://doi.org/10.1016/j.geomorph.2015.07.010.

U.S. Department of Interior, Bureau of Reclamation. (2015). Bank Stabilization Design Guidelines. Report No. SRH-2015-25. 319pp.

U.S. Geological Survey. (2017). 5 Meter Alaska Digital Elevation Models (DEMs)-USGS National Map 3DEP Downloadable Data Collection. U.S. Geological Survey, 2017. Available online: https://www.sciencebase.gov/catalog/item/5641fe98e4b0831b7d62e758 (accessed on 19 May 2023).

U.S. Geological Survey. (2023). Watershed Boundary Dataset, U.S. Geological Survey, U.S. Department of Interior. Available online: https://www.usgs.gov/national-hydrography/watershed-boundary-dataset (accessed on 28 May 2023).

U.S. Geological Survey. (2025). National Geospatial Program Standard and Specifications: Elevation-Derived Hydrography Data Acquisition Specifications 2024 Revision A3, 167 pp.

U.S. Geological Survey. (2026). USGS 3D Hydrography Program (3DHP) Downloadable Datasets 2025. https://www.sciencebase.gov/catalog/item/6930876ed4be027594fed169

Xiao, X., Chen, J., Chen, D., Chen, R. (2019). Effects of river sinuosity on the self-purification capacity of the Shiwuli Rivers, China. Water Supply, 19(4), 1152-1159. https://doi.org/10.2166/ws.2018.166

Xiao, C., Chai, Z., Chen, D., Luo, Z., Li, Y., Ou, Q., Zhang, Y. (2025). Research on the influence of river morphological changes on water self-purification capacity: A case study of the Shiwuli River in Chaohu Basin. Water, 17(11), 1694. https://doi.org/10.3390/w17111694

Yu, Z., Fu, Y., Zhang, Y., Liu, Z., & Liu, Y. (2023). Quantifying the impact of changes in sinuosity on river ecosystems. Water, 15(15), 2751. https://doi.org/10.3390/w15152751

Zhu, L., Chen, D., Hassan, M. A., &Venditti, J. G. (2022). The influence of riparian vegetation on the sinuosity and lateral stability of meandering channels. Geophysical Research Letters,49, e2021GL096346. https://doi.org/10.1029/2021GL096346